Electron-impact-induced dissociation of small argon clusters

Thomas Pflüger,[1,2,*] Xueguang Ren,[1,2,†] and Alexander Dorn[2]
[1]*Physikalisch-Technische Bundesanstalt, Bundesallee 100, 38116 Braunschweig, Germany*
[2]*Max-Planck-Institut für Kernphysik, Saupfercheckweg 1, 69117 Heidelberg, Germany*
(Received 7 April 2015; published 6 May 2015)

We study electron-impact-induced dissociation of small van der Waals–bound argon complexes at a projectile energy of 120 eV. Kinetic-energy-release (KER) spectra of the Ar_2 and Ar_3 parent species for the final charge states $2Ar^+$, $Ar^+ + Ar^{2+}$, and $Ar_2^+ + Ar^+$ and electron energies have been measured together with angular distributions of fragment ions. They are used to identify dissociation mechanisms such as interatomic Coulombic decay (ICD).

DOI: 10.1103/PhysRevA.91.052701 PACS number(s): 34.80.Gs

I. INTRODUCTION

The study of van der Waals complexes has been a quickly developing field in recent years. Specifically, ionization and fragmentation dynamics have been investigated extensively (e.g., [1–4]). Furthermore, mechanisms for relaxation were proposed for clusters that could not be seen for the corresponding monomer. The most prominent—dubbed interatomic Coulombic decay, or ICD—has been found to be a very efficient and fast process that was first predicted theoretically [5] and later demonstrated experimentally in neon clusters and in neon dimers [6,7]. Briefly, ICD can occur in loosely bound systems (like dimers) by means of an inner valence vacancy, where, in a purely atomic system, filling this hole with a valence electron is not sufficient to eject another valence electron to the continuum. However, the transition energy can be sufficient to ionize a neighboring atom, which, in the case of dimers, results in two charged fragments that Coulomb explode.

Since its discovery, a variety of processes involving ICD, which finally lead to dissociation, have been found. Apart from direct ICD, where the neighboring site is ionized by a virtual photon as described by Cederbaum *et al.* [5], the ionization can also be accomplished by filling the inner-shell vacancy by a valence electron from the neighboring site (exchange ICD) [8]. Similarly, ionization can occur by electron transfer to a core vacancy while ejecting a valence electron from the donor site (electron-transfer-mediated decay or ETMD) [9,10]. Figure 1 shows a schematic depiction of the described processes.

Recently it was found that in dimers such as Ar_2, where an inner valence hole is energetically insufficient for ICD, it can occur nevertheless after a cascade of one-site Auger processes triggered by core-hole ionization. Such a mechanism will prepare the dimer in an excited one-site doubly ionized state that will decay via ICD into a triply ionized final state [11,12]. Furthermore, in a series of theoretical and experimental investigations it was found that ICD can be triggered by an initial core excitation followed by a resonant Auger decay [13–16]. This process will leave the dimer in a doubly ionized final state.

Experimentally, in all of the described investigations, ionization was achieved using high-energy photons from synchrotron radiation or free-electron lasers to create core vacancies which decay to states leading to ICD. Rarely studied is the use of massive particles to invoke ICD (e.g., [17]). Experiments involving electrons as projectiles were, until now, limited to detection of the fragment ion only [18]. In part this is due to the low cross sections for inner-shell ionization. Compared to core ionization, ionization/excitation processes exhibit larger cross sections and are therefore easily accessible by electron impact.

Another interesting point about ICD is that it is found to be an efficient source of low-energy electrons. For example, the prominent $Ne_2^+(2s^{-1})$ decay produces electrons of <2 eV. At the same time, efficient production of low-energy electrons has gained significant interest in medicinal sciences owing to their role in radiation-induced production of DNA double-strand breaks [19–21].

In this work we investigate decay mechanisms in argon dimers and trimers following electron-impact ionization. This is achieved by measuring the three-dimensional momentum vectors of argon ions of different charge states and electrons in coincidence. More precisely, the experiment was carried out with a projectile energy of $E_0 = 120$ eV. This ensures that both $2p$ ionization and $2p$ excitation (e.g., $2p \rightarrow 3d$) can be excluded since their threshold energies are $\gtrsim$250 eV. By analyzing kinetic-energy-release (KER) spectra and the energy distribution of the ejected electrons, detailed information about the underlying mechanisms can be gained. The aim is to see whether mechanisms like ICD, which have previously been invoked by Auger decays through either core-hole ionization or excitation, can be prepared directly by electron impact.

The structure of this article is as follows. In Sec. II a brief overview of the experimental setup as well as the method is given. The results are discussed in detail in Sec. III, and a Summary and Conclusions can be found in Sec. IV.

II. EXPERIMENTAL SETUP

This work has been carried out by employing an advanced reaction microscope specially modified for electron-impact studies [22,23]. Briefly, imaging of the charged fragments onto time- and position-sensitive detectors is achieved by homogeneous electric and magnetic fields. These fragments are created by crossing a pulsed projectile electron beam, propagating along the spectrometer axis, with a cold target beam, created by a supersonic expansion of the gas under investigation (see

*thomas.pflueger@ptb.de
†ren@ptb.de

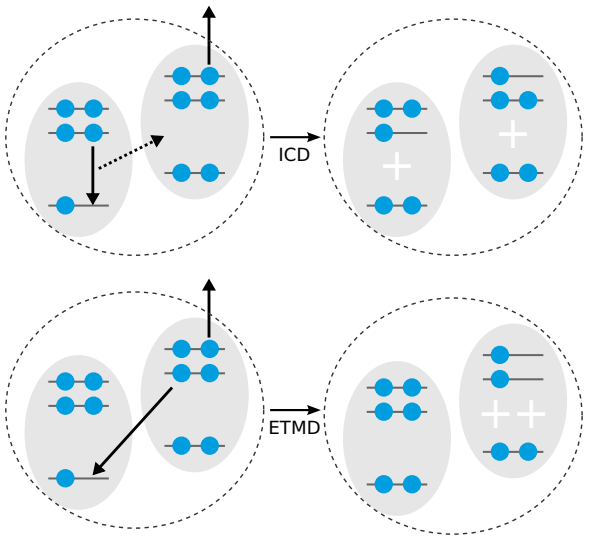

FIG. 1. (Color online) Simplified representation of different processes. While ICD (top) involves energy transfer between the constituents via a virtual photon, ETMD (bottom) is driven by electron exchange (after Ref. [9]).

Fig. 2). Since fragments resulting from Coulombic explosion can gain substantial momenta [$O(100$ a.u)], they can escape the spectrometer if they are emitted perpendicular to the spectrometer axis. This effect can be reduced by increasing the extraction field with the drawback that the electron energy resolution will suffer. Hence, the ion side of the spectrometer has been shortened with respect to the electron side to reduce the time-of-flight (TOF) of heavy fragments and, in turn, increases their acceptance. For this work, the dimensions for the electron's and ion's acceleration lengths were $a_e = 11$ cm and $a_i = 4$ cm, respectively, while a time-focusing condition, where the drift length amounts to 2 times the acceleration's length, was employed for both sides. From time and position information, the three-dimensional momentum vector of each charged particle can be calculated.

The necessity of a magnetic field requires the projectile beam to be injected on-axis, which, in turn, calls for a central hole in the ion detector. The electron detector, on the other hand, has a hole only through the microchannel plate. The position-sensitive anode serves as a beam dump.

For the projectile creation a thermocathode was biased to a negative potential and a positive nanosecond voltage pulse was applied to a slightly negatively biased Wehnelt cylinder.

Cluster production was achieved by expanding argon through a 30-μm nozzle with a backing pressure of 3 bar at room temperature. The temperature after expansion was estimated to be $T_f \sim 0.9$ K.

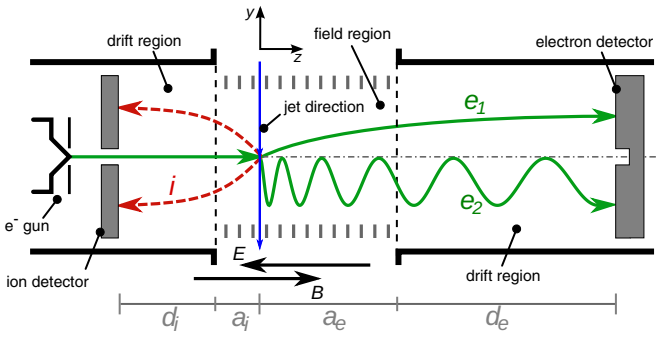

FIG. 2. (Color online) Schematic view of the apparatus. The bottom rule marks $d_{i,e}$ and $a_{i,e}$, the lengths of the drift and acceleration regions for ions and electrons, respectively. Arrow E indicates the direction of the electric field and arrow B the magnetic field.

III. RESULTS AND DISCUSSION

In a first step of studying dissociation processes of small argon clusters we present a TOF coincidence map in Fig. 3, where the TOFs of two detected ions are plotted against each other. It shows correlation structures between two ions in the form of lines having negative slopes. For the $Ar^{2+} + Ar^{+}$ coincidence region, as well as for $Ar^{+} + Ar^{+}$ and $Ar_2^{+} + Ar^{+}$, sharp line-structures indicate a two-body process where the parent cluster dissociates into two ions, both of which are detected. In contrast, broad tilted structures imply missing momenta originating from dissociation into three or more fragments. This can mean the creation of a neutral fragment which cannot be detected, or the creation of three or more charged fragments which all may have been detected but of which only two are displayed. The horizontal and vertical structures originate from false coincidences. We estimate the amount of dimers in the gas jet to be on the order of 1%; hence, the probability for ionization events of atomic argon is high. False coincidences are created by detecting those events together with fragment ions from the dissociation of argon clusters. They mark the positions for nondissociative events of the respective species (e.g., $Ar \rightarrow Ar^{2+}$).

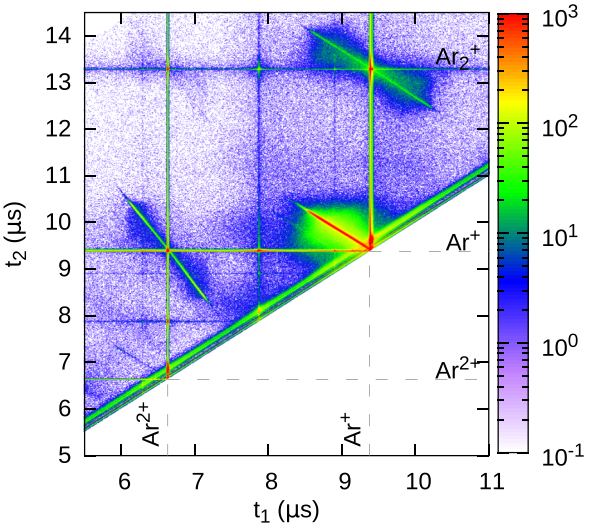

FIG. 3. (Color online) Ion-ion coincidence map. Peak structures with negative slopes indicate coincident ion events from two-body breakup. Horizontal and vertical structures correspond to false coincidences. The labels show the positions of the nondissociative ionization peaks. Noteworthy is the region of the $Ar_2^{+} + Ar^{+}$ coincidence. The sharp line structure originates from direct Ar_3 breakup, while the background is the result of the breakup of a larger parent cluster.

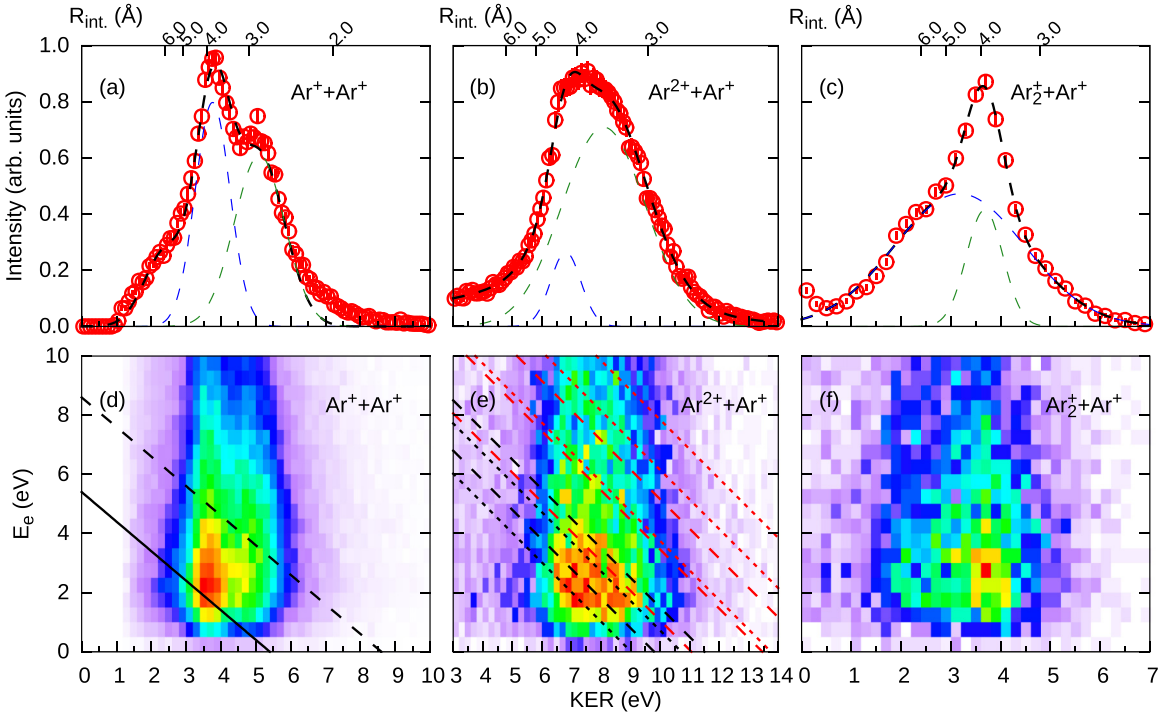

FIG. 4. (Color online) KER spectra for $Ar^+ + Ar^+$ (a), $Ar^{2+} + Ar^+$ (b), and $Ar_2{}^+ + Ar^+$ (c) coincidences. The top scales show the internuclear distance R_{int} in angstroms. Dashed curves are Gaussian fits. KER vs electron energy for $Ar^+ + Ar^+$ (d), $Ar^{2+} + Ar^+$ (e), and $Ar_2{}^+ + Ar^+$ (f) coincidences. The dashed and dotted lines in (d) and (e) indicate constant sum energies $E_e + E_{\text{KER}}$ (see text).

The interesting region of the $Ar_2{}^+ + Ar^+$ coincidence is composed of two different contributions. Foremost, a sharp line-structure is visible on top of a broad, but still tilted background. While, as explained above, the sharp structure is the result of the two-body breakup of an argon trimer into a dimer and a monomer ion ($Ar_3 \rightarrow Ar_2{}^+ + Ar^+$), the background stems from the breakup of a larger parent cluster, like a quadromer, into three or more fragments (e.g., $Ar_4 \rightarrow Ar_2{}^+ + Ar^+ + Ar$). At the same time, no evidence was found for a quadromer breakup into two dimer ions. A similar feature, where a sharp line sits on top of a broader background, can be observed for the $2Ar^+$ coincidence, where part of the broad background can be attributed to the trimer breaking up into three singly charged argon ions, of which only two are plotted.

In Fig. 4 the top row shows KER spectra while the bottom row shows the KER against the electron energy for the three most prominent final states, respectively: $Ar_2 \rightarrow 2Ar^+$ (a), (d), $Ar_2 \rightarrow Ar^{2+} + Ar^+$ (b), (e), and $Ar_3 \rightarrow Ar_2{}^+ + Ar^+$ (c), (f). Additionally, the top scale of each panel shows the calculated internuclear distance at the instance of Coulomb explosion, assuming that $E_{\text{kin}} \propto 1/R_{\text{int}}$. In the following, we will discuss each final state individually.

A. Doubly charged final state

The KER spectrum in Fig. 4(a) shows the dissociation into two singly charged argon ions. An interesting observation is the appearance of two main peaks at 3.76 eV ($\hat{=}$3.83 Å) and 5.10 eV ($\hat{=}$2.87 Å), respectively. Comparing these values to the internuclear distance of the neutral dimer $R_{\text{int.}}(Ar_2) =$ 3.77 Å (see [24]), we can deduce that in the former case the dimer dissociates without significant nuclear motion while in the latter case it contracts significantly before Coulombic explosion occurs. Another way of describing the aforementioned is that the process leading to the peak at 3.76 eV takes place immediately while for the peak at 5.10 eV the two cores have time to move towards each other.

There are three principle pathways that can result in a doubly charged ionic final state:

$$e^- + Ar_2 \rightarrow \begin{cases} Ar_2{}^{+*} + 2e^- \rightarrow 2Ar^+(3p^{-1}) + 3e^-, & (1) \\ Ar_2{}^{2+} + 3e^- \rightarrow 2Ar^+(3p^{-1}) + 3e^- + h\nu, & (2) \\ 2Ar^+(3p^{-1}) + 3e^-. & (3) \end{cases}$$

Equation (1) represents the aforementioned ICD channel. The one-site excited state of the cation decays under emission of a (slow) electron to the repulsive potential curve. The signature for this channel resides in the fact that the emitted electron and the KER share the total energy of the initial state; hence, they are correlated. A one-site dicationic state can undergo a radiative transition to the dissociative state, where one of the vacancies is filled by a neighboring valence electron while the excess energy is carried by a photon as shown by Eq. (2). Naturally, such a process requires the dimer to contract in order to maximize the overlap of wave functions. Lastly, the simplest reaction, depicted in Eq. (3), is the direct population of the repulsive $2Ar^+(2p^{-1})$ potential curve, where one electron is removed from each constituent. Judging from the large internuclear distance, it is assumed that the probability for such an event should depend on the orientation of the dimer with respect to the projectile direction.

Since ICD in argon dimers relies on the population of satellite states (as compared to excitation of the cation by

direct inner-valence ionization), two distinct groups of such states can be found: lower-lying states with long vibrational periods and short ICD lifetimes, and higher-lying states with short vibrations periods and long ICD lifetimes. The former will result in low KER peaks, while the latter will result in high KER peaks due to the contraction of the dimer. Recently, Kimura and co-workers performed an experiment where the initial Auger cascade was initiated by photoexcitation rather than inner-shell ionization [15]. Also, here an Auger decay leads to two vacancies in the M shell. Their findings clearly show two peaks in the KER spectrum at 3.8 and 5.2 eV, respectively, very close to the values reported here. A theoretical investigation by Miteva *et al.* concludes that the lower KER value originates from fast ICD transitions of lower-lying excited states of the dimer cation [$Ar^+(3p^{-2}3d)$ and $Ar^+(3p^{-2}4s)$], while the higher KER value stems from higher excited states [$Ar^+(3p^{-2}4d)$ and $Ar^+(3p^{-2}5s)$] [25]. For the former states the ICD lifetime is found to be an order of magnitude shorter than the vibrational period of the excited states. Consequently, nuclear dynamics is negligible and the dissociation takes place at the neutral internuclear distance. For the higher excited states the situation is reversed and the cation undergoes nuclear motion before ICD, resulting in a higher KER value. Here, the transition occurs with a high probability at the position of the inner turning point of the potential energy curve. It is important to note that the initial core excitation and the subsequent resonant Auger decay are considered to be instantaneous. Consequently, a direct population of the excited ICD initial states is believed to yield the same results, although the population of various angular momentum states of the configuration $3p^{-2}nl$ might be different for electron impact. A closer look at the correlation between KER and electron energy [Fig. 4(d)] supports our arguments: for the lower KER of 3.76 eV lower energetic states are excited and electron energy peaks at roughly $E_e = 2$ eV, while the for a KER of 5.10 eV the involved states are energetically higher and, hence, the electron energy is higher.

In general, ICD manifests itself in a correlation between the KER and the energy of the ejected electron E_e. Figure 4(d) shows such a spectrum with the dashed and dotted lines corresponding to constant energy sums $E_e + E_{\mathrm{KER}} = 5.4$ eV for a $Ar^{2+}(3p^{-3}\,{}^1D\,3d\,{}^2D)$ + Ar initial state (dashed) and the $E_e + E_{\mathrm{KER}} = 8.6$ eV $Ar^{2+}(3p^{-3}\,{}^1D\,4d\,{}^2D)$ + Ar initial state (dotted). Since we are not bound by the population of specific Auger final states, we attribute the lack of correlation to a large number of ICD states that are populated by the initial projectile interaction.

A process corresponding to Eq. (2) was found in previous photoabsorption experiments in which Coulombic explosion was achieved in argon dimers by creating a $2p$ core hole, which decays through a one-site *LMM* Auger decay, creating two vacancies in the M shell. The KER spectra show only a single peak at 5.2 eV which corresponds to a small internuclear distance (2.7 Å) [11]. At the same time no significant amount of low-energy electrons could be observed. Since this observation rules out ICD as a possible mechanism, it is concluded that the dimer ion dissociates after radiative charge transfer from doubly charged states $Ar^{2+}(3p^{-2})$ + Ar. Since for the present projectile energy of 120 eV $2p$ ionization is energetically not accessible (the ionization potential is about ∼250 eV [26]), this pathway is not possible. However, the direct preparation of a one-site doubly ionized state is possible and has a total cross section of 2.79×10^{-17} cm^2, of which the main contribution is the population of the $(3p^{-2})$ state with a partial cross section of 2.48×10^{-17} cm^2 [27].

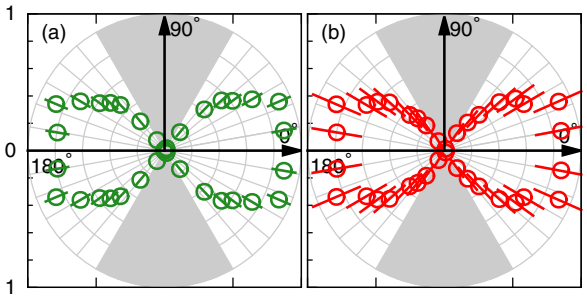

FIG. 5. (Color online) Angular distribution of the Ar^+ fragments in the laboratory frame for a KER of 3.76 eV (a) and 5.10 eV (b). The zero degrees direction coincides with the projectile direction. The gray shaded area marks a region of reduced acceptance.

The second possibility for the peak at a large KER of 3.76 eV in Fig. 4(a) can also arise by direct population of the repulsive state, as indicated by Eq. (3). The probability for a direct coupling should depend strongly on the orientation of the molecular axis with respect to the projectile direction, since it would require two subsequent interactions at both sites of the dimer. This, in turn, should be more likely if the axis is aligned in parallel with the projectile beam. Monte Carlo simulations for ion collision experiments show that direct population of the repulsive state favors a pronounced dipole distribution of the ionic fragments, whereas secondary processes like ICD contribute to an isotropic distribution [28]. In Fig. 5, the angular distributions of the Ar^+ fragments are plotted for the KER 3.76 eV (a) and 5.10 eV (b). As one can see, both channels exhibit dipolar patterns aligned along the projectile direction.

B. Triply charged final state

The triply ionized final state in Fig. 4(b) shows a single peak located at 7.42 eV (≙3.88 Å), which coincides with the neutral dimer internuclear distance. This agrees with results from Ueda *et al.* for $2p$ photoionization, where for the triply ionized final state the sole contribution to the KER is found at 3.7 Å. In their work, a correlation between the KER and low-energy electrons was found, giving a strong indication of ICD as the prominent decay mechanism [11]. They concluded that ICD is enabled after an Auger decay to excited $Ar^{2+}(3p^{-3}3d)$ + Ar states (^3P and ^1P) which result in electron energies of 3.8 eV and 2.1 eV for transitions from ^1P. For electron impact, these Auger final states are expected to be directly accessible [together with various other $(3p^{-3}nl)$ states]. Theoretically, such a mechanism—where ICD is triggered from a one-site dicationic state—was predicted by Santra and Cederbaum for the neon dimer [29]. For a fast decay mechanism such as ICD, one has to look at the correlation between the KER and low energetic electrons shown in Fig. 4(e). In such a process, the ions and the ICD electron share the excess energy. The negatively sloped black dashed lines indicate the sum energy of

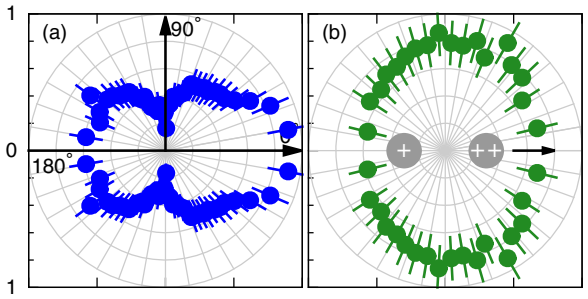

FIG. 6. (Color online) (a) Angular distribution of the Ar^{2+} fragments in the laboratory frame for the $Ar^{2+} + Ar^{+}$ final state. The zero degrees direction coincides with the projectile direction. (b) Angular distribution of electrons with energies <4 eV in the molecular frame.

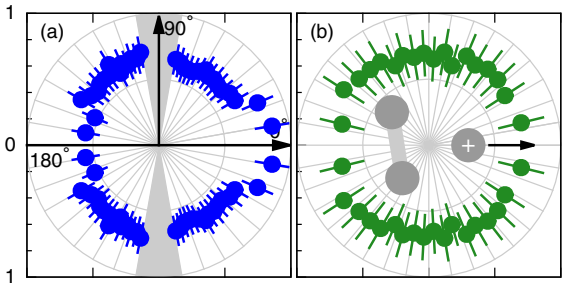

FIG. 7. (Color online) (a) Angular distribution of the Ar^{+} fragments in the laboratory frame for the $Ar_2^{+} + Ar^{+}$ final state of Ar_3 ionization. The zero degrees direction coincides with the projectile direction. The gray shaded area marks a region of reduced acceptance. (b) Angular distribution of electrons with energies <5 eV with respect to the Ar^{+} momentum vector.

$E_e + E_{\mathrm{KER}} = 9.8$ eV for an $Ar^{2+}(3p^{-2}\,{}^1D) + Ar^{+}(3p^{-1}\,{}^2P)$ final state and $E_e + E_{\mathrm{KER}} = 11.5$ eV for an $Ar^{2+}(3p^{-2}\,{}^3P) + Ar^{+}(3p^{-1}\,{}^2P)$ final state after ICD, respectively, starting from the ^1P state. The black dotted lines indicate the two respective channels starting from the ^3P state with sum energies of $E_e + E_{\mathrm{KER}} = 9.0$ eV and $E_e + E_{\mathrm{KER}} = 10.7$ eV, respectively. Furthermore, in red, decays from two additional initial states are considered, which are $Ar^{2+}(3s^{-2}\,{}^1S) + Ar$ (dashed) and $Ar^{2+}(3p^{-3}\,{}^2D\,4d\,{}^3P) + Ar$ (dotted). As one can see in Fig. 4(e), there is such a correlation for the main contribution to the spectrum around 2 eV electron energy, where compared to experiments relying on Auger decays to populate the ICD states, four of the assumed ten channels contribute, creating a broad band. There even seems to be a faint signature for sum energies corresponding to an initial $3s$ (red, dashed) double ionization as well as a $4d$ (red, dotted) excitation at around $E_e = 8$ eV.

Besides a secondary decay process, direct population of the triply charged final state is possible for electron-impact ionization. Due to the large internuclear distance of the neutral dimer, it can be reached only by sequentially ionizing both constituents. For the direct preparation, the ionization potential is 66.85 eV and corresponds to the creation of $Ar^{2+}(3p^{-2}) + Ar^{+}(2p^{-1})$. As mentioned above, the cross section for double ionization is $\sigma(3p^{-2}) = 2.48 \times 10^{-17}$ cm^2 while the single ionization cross section is $\sigma(3p^{-1})_{\mathrm{max}} = 2.73 \times 10^{-16}$ cm^2 at 49.5 eV impact energy [27]. The probability for sequential ionization should, as for the doubly ionized final state, depend on the angular orientation of the dimer.

In Fig. 6 the angular distributions of the doubly charged fragments Ar^{2+} in the laboratory frame (a) as well as the angular distribution in the molecular frame of electrons below 4 eV kinetic energy (b) are shown. The angular acceptance covers almost the complete polar range from 180° to 0°, since the two fragments have different m/q ratios and, therefore, no detector dead times occur. As one can see from the ion distribution, there is a pronounced tendency for Ar^{2+} emission along the projectile direction, while in the vicinity of 90° the distribution does not go to zero. We can conclude that the dimer is ionized preferentially when being oriented in parallel with the projectile beam, pointing to the sequential mechanism. Since the intensity in the perpendicular orientation only dropped by half, there is still a significant contribution which is not dependent on the orientation. The anisotropy in the angular distribution can, on the other hand, also be an indication of transition probabilities depending on the direction of the momentum transfer with respect to the molecular orientation [30]. The electron emission in the molecular frame is essentially isotropic.

C. Doubly charged final state of the trimer

Lastly, Fig. 4(c) shows the KER spectrum for the doubly ionized final state of the argon trimer. Its structure is reported to be an equilateral triangle with a bond length of 3.8 Å [31,32]. The reflection principle to deduce the internuclear distance from the KER therefore cannot be applied in a straightforward way since it is expected that the manner of the breakup introduces complicated dynamics, where the KER is partly transferred to rotational energy of the Ar_2^{+} fragment. It is, however, interesting to note that the main peak is found at 3.68 eV. On the other hand, there is also a lesser pronounced side peak at smaller KER values that indicates more complex, multistep dissociation scenarios.

Consequently, the angular distribution of the electrons in the frame of the Ar^{+} ionic fragment's momentum vector [see Fig. 7(b)] does not exhibit any structure and shows isotropic behavior. The ionic angular distribution in the laboratory frame [Fig. 7(a)], on the other hand, shows a distinctly different distribution from, e.g., the triply charged dimer case. Here the intensity is largest for the 0° and the 90° direction with smaller peaks in the 45° and 135° directions. Whether this can be attributed to a preferred orientation for this decay channel, for the time being, cannot be answered conclusively. One can, however, assume that, as stated above, the transition probability depends on the orientation of the molecular orbitals with respect to the momentum transfer direction.

IV. CONCLUSIONS

We have measured dissociative electron-impact ionization on argon dimers and trimers at a projectile energy of 120 eV. Three main reaction channels were found, namely, the doubly and triply charged final states of the dimer as well as the doubly charged final state of the trimer. For all three channels KER and electron energies were measured. The Ar_2^{2+} channel

reveals two major contributions to the KER spectrum, where one was assigned to be a combination of direct dissociation and fast ICD, while the latter process could not be unambiguously identified, mainly due to the large number of possible excited states that can be populated by electron impact. The second peak is also assigned to an ICD process which takes place after severe contraction of the intermediate dimer ion at the position of the inner turning point of the potential energy curve. Similar KER spectra where observed experimentally and found theoretically, where in the experiments ICD states were prepared by one-site photoexcitation followed by resonant Auger decay. Since a contribution of a radiative process cannot be ruled out, further investigation is needed. In our study, the Ar_2^{3+} channel revealed a signature for ICD with contributions of several directly populated excited states of the intermediate dimer dication, which was observed unambiguously for the first time in an electron collision experiment. The acquired ionic angular distribution also contains indications for a direct sequential ionization.

The dissociation of argon dimers and trimers by electron impact reveals that ultrafast decay mechanisms like ICD are not exclusive to interaction with high energetic photons. Furthermore, the present experiment demonstrates that electron impact can prepare the dimer in a one-site excited state directly without an intermediate decay mechanism.

ACKNOWLEDGMENT

T.P. would like to thank K. Gokhberg for his helpful remarks.

[1] U. Buck and H. Meyer, J. Chem. Phys. **84**, 4854 (1986).
[2] A. Bastida, N. Halberstadt, J. A. Beswick, F. X. Gadéa, U. Buck, R. Galonska, and C. Lauenstein, Chem. Phys. Lett. **249**, 1 (1996).
[3] Y. Morishita, X.-J. Liu, N. Saito, T. Lischke, M. Kato, G. Prümper, M. Oura, H. Yamaoka, Y. Tamenori, I. H. Suzuki, and K. Ueda, Phys. Rev. Lett. **96**, 243402 (2006).
[4] K. Schnorr *et al.*, Phys. Rev. Lett. **111**, 093402 (2013).
[5] L. S. Cederbaum, J. Zobeley, and F. Tarantelli, Phys. Rev. Lett. **79**, 4778 (1997).
[6] S. Marburger, O. Kugeler, U. Hergenhahn, and T. Möller, Phys. Rev. Lett. **90**, 203401 (2003).
[7] T. Jahnke, A. Czasch, M. S. Schöffler, S. Schössler, A. Knapp, M. Käsz, J. Titze, C. Wimmer, K. Kreidi, R. E. Grisenti, A. Staudte, O. Jagutzki, U. Hergenhahn, H. Schmidt-Böcking, and R. Dörner, Phys. Rev. Lett. **93**, 163401 (2004).
[8] K. Kreidi *et al.*, J. Phys. B: At., Mol., Opt. Phys. **41**, 101002 (2008).
[9] J. Zobeley, R. Santra, and L. S. Cederbaum, J. Chem. Phys. **115**, 5076 (2001).
[10] K. Sakai, S. Stoychev, T. Ouchi, I. Higuchi, M. Schöffler, T. Mazza, H. Fukuzawa, K. Nagaya, M. Yao, Y. Tamenori, A. I. Kuleff, N. Saito, and K. Ueda, Phys. Rev. Lett. **106**, 033401 (2011).
[11] K. Ueda, X.-J. Liu, G. Prümper, H. Fukuzawa, Y. Morishita, and N. Saito, J. Electron Spectrosc. Relat. Phenom. **155**, 113 (2007).
[12] N. Saito, Y. Morishita, I. H. Suzuki, S. D. Stoychev, A. I. Kuleff, L. S. Cederbaum, X.-J. Liu, H. Fukuzawa, G. Prümper, and K. Ueda, Chem. Phys. Lett. **441**, 16 (2007).
[13] F. Trinter, M. S. Schoffler, H.-K. Kim, F. P. Sturm, K. Cole, N. Neumann, A. Vredenborg, J. Williams, I. Bocharova, R. Guillemin, M. Simon, A. Belkacem, A. L. Landers, T. Weber, H. Schmidt-Bocking, R. Dorner, and T. Jahnke, Nature (London) **505**, 664 (2014).
[14] K. Gokhberg, P. Kolorenc, A. I. Kuleff, and L. S. Cederbaum, Nature (London) **505**, 661 (2014).
[15] M. Kimura, H. Fukuzawa, K. Sakai, S. Mondal, E. Kukk, Y. Kono, S. Nagaoka, Y. Tamenori, N. Saito, and K. Ueda, Phys. Rev. A **87**, 043414 (2013).
[16] P. O'Keeffe, E. Ripani, P. Bolognesi, M. Coreno, M. Devetta, C. Callegari, M. Di Fraia, K. C. Prince, R. Richter, M. Alagia, A. Kivimäki, and L. Avaldi, J. Phys. Chem. Lett. **4**, 1797 (2013).
[17] H.-K. Kim, H. Gassert, M. S. Schöffler, J. N. Titze, M. Waitz, J. Voigtsberger, F. Trinter, J. Becht, A. Kalinin, N. Neumann, C. Zhou, L. P. H. Schmidt, O. Jagutzki, A. Czasch, H. Merabet, H. Schmidt-Böcking, T. Jahnke, A. Cassimi, and R. Dörner, Phys. Rev. A **88**, 042707 (2013).
[18] S. Yan, P. Zhang, X. Ma, S. Xu, B. Li, X. L. Zhu, W. T. Feng, S. F. Zhang, D. M. Zhao, R. T. Zhang, D. L. Guo, and H. P. Liu, Phys. Rev. A **88**, 042712 (2013).
[19] B. Boudaïffa, P. Cloutier, D. Hunting, M. A. Huels, and L. Sanche, Science **287**, 1658 (2000).
[20] M. Mucke, M. Braune, S. Barth, M. Forstel, T. Lischke, V. Ulrich, T. Arion, U. Becker, A. Bradshaw, and U. Hergenhahn, Nat. Phys. **6**, 143 (2010).
[21] W. Iskandar, J. Matsumoto, A. Leredde, X. Fléchard, B. Gervais, S. Guillous, D. Hennecart, A. Méry, J. Rangama, C. L. Zhou, H. Shiromaru, and A. Cassimi, Phys. Rev. Lett. **114**, 033201 (2015).
[22] J. Ullrich, R. Moshammer, A. Dorn, R. Dörner, L. P. H. Schmidt, and H. Schmidt-Böcking, Rep. Prog. Phys. **66**, 1463 (2003).
[23] M. Dürr, C. Dimopoulou, A. Dorn, B. Najjari, I. Bray, D. V. Fursa, Z. Chen, D. H. Madison, K. Bartschat, and J. Ullrich, J. Phys. B: At., Mol., Opt. Phys. **39**, 4097 (2006).
[24] K. Patkowski, G. Murdachaew, F. Cheng-Ming, and K. Szalewicz, Mol. Phys. **103**, 2031 (2005).
[25] T. Miteva, Y.-C. Chiang, P. Kolorenč, A. I. Kuleff, K. Gokhberg, and L. S. Cederbaum, J. Chem. Phys. **141**, 064307 (2014).
[26] G. C. King, M. Tronc, F. H. Read, and R. C. Bradford, J. Phys. B: At., Mol., Opt. Phys. **10**, 2479 (1977).
[27] L. K. Jha, S. Kumar, and B. N. Roy, Eur. Phys. J. D **40**, 101 (2006).
[28] H.-K. Kim *et al.*, Phys. Rev. A **89**, 022704 (2014).
[29] R. Santra and L. S. Cederbaum, Phys. Rev. Lett. **90**, 153401 (2003).
[30] G. H. Dunn, Phys. Rev. Lett. **8**, 62 (1962).
[31] P. J. Kuntz and J. J. Hogreve, J. Chem. Phys. **95**, 156 (1991).
[32] T. Gonzalez-Lezana, J. Rubayo-Soneira, S. Miret-Artes, F. A. Gianturco, G. Delgado-Barrio, and P. Villarreal, J. Chem. Phys. **110**, 9000 (1999).